TECHNISCHE MECHANIK, 32, 2-5, (2012), 416 - 424
submitted: October 13, 2011

Optimisation of the Explosive Compaction Process for Powder-In-Tube MgB_2 Superconductors Using Numerical Simulations

A. G. Mamalis, I. D. Theodorakopoulos and A. K. Vortselas

High quality, ex-situ powder-in-tube (PIT) MgB_2 superconductors are fabricated using the explosive compaction technique. During the treatment, the precursor materials are densified under high strain-rates using PETN as the explosive medium. It has been found that the product quality depends on the porosity of the compact, which affects the critical current density of the superconductor by introducing changes in the interparticle bonding of the material, as well as the peak shockwave pressure which has an effect on the maximum tensile stress imposed to the specimen. This determines the crack formation in the consolidated powder and the uniformity of the product's final shape. The explosive compaction process has been modeled using the LS-DYNA explicit finite element code where the compacted MgB_2 powder is treated as a porous soil-like material with a customised yield surface. The results of the numerical simulation include the compact porosity, the pressure, the temperature and strain rate profiles as well as the dimensions of the final product, which are used as input data in order to assess the efficiency of the explosive compaction process. The process is non-parametrically optimised for the above mentioned quality factors, and the optimal dimensions of the explosive charge and container tube are determined.

1 Introduction

Nowadays, superconductivity has a significant impact on many technological sectors, for example in the production of electric motors and magnetic sensors as well as in the energy transmission and storage technology. Superconducting wires and tapes are the key product for the adoption of this high technology, but the selection of a suitable superconducting material is not an easy task. MgB_2 is in general a low cost superconductor compared to other ceramic high T_c materials, with a transition temperature near the liquid hydrogen boiling point. It has been estimated that approximately 15% of the generated electricity is dissipated during power transportation. In that respect, MgB_2 can be used for the construction of zero loss superconducting transmission lines, where liquid hydrogen may serve as refrigeration medium. The production of wires, coils and tapes requires forming at very high pressures due to the poor formability of the extremely hard ceramic superconductors. For this reason, the powder-in-tube (PIT) explosive compaction technique is considered to be a very promising powder metallurgy forming process for the fabrication of near full density MgB_2 superconductors as given in Mamalis et al. (2009).

The present work is concerned with the optimization of the explosive compaction process, incorporating MgB_2 powders. The optimization is performed on an LS-DYNA numerical simulation model of the explosive compaction, where the external diameter of the tube and the dimensions (length and diameter) of the explosive surrounding of the PIT are used as input parameters. The peak pressure, peak maximum principal stress, porosity, uniformity of the tube radius, and mass of the explosive, are the corresponding simulation outputs, with the porosity being the most important parameter to optimize, since it is directly related to the interparticle bonding of the compact which affects the critical current density of the superconductor.

2 Numerical Simulation of Explosively Densified PIT MgB_2 Powders

The shock consolidation process of the superconducting powders is numerically simulated using the LSDYNA finite element code. Since the PIT sample deformation during explosive loading is considered to be axisymmetric, a quarter 3D explicit finite element model is developed which is sufficient to accurately simulate the compaction procedure reducing this way the computational time. The finite element model mesh together with the corresponding experimental setup are demonstrated in Figures 1 (a-d). It consists of the explosive

medium, the steel container, the MgO fillers, the PE caps and the MgB_2 powders located at the center of the tube. Figure 1 (d) illustrates the final shape of the compacted powders inside the tube, where it may be observed that after the densification, the MgB_2 powder compact is approximately of cylindrical geometry. On the contrary, the edges of the compact have been heavily deformed which is attributed to the interactions of the shock waves generated by the explosion. This can be explained by the fact that the waves reflect in the form of compressive/tensile stress pulses and at the same time overlap at these two locations, which causes the material to be deformed in an irregular manner.

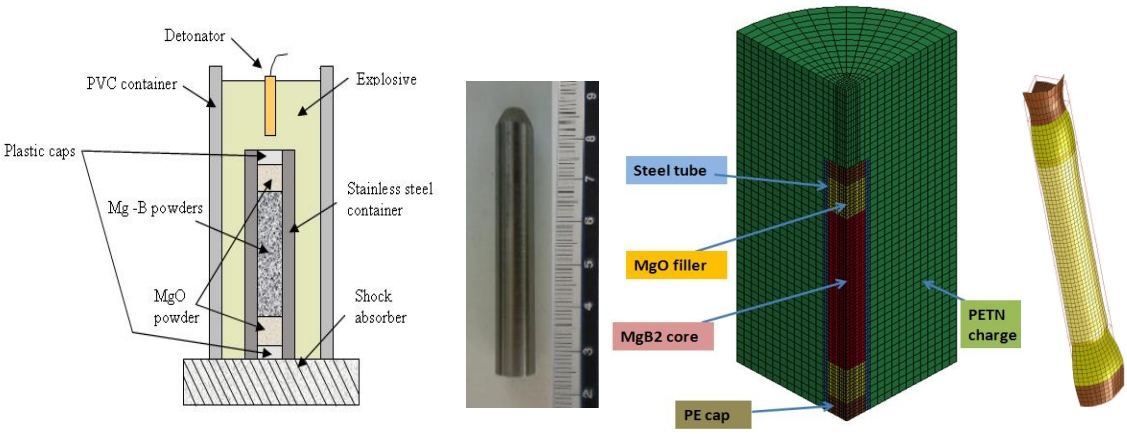

(a) (b) (c) (d)

Figure 1. (a) Experimental setup; (b) Compacted MgB_2 core; (c) Finite element model mesh; (d) Final tapered shape of the compacted material inside the tube

Three material models are selected to address the different properties of the three main parts of the PIT. In particular, the PETN explosive, the steel container and the MgB_2 and MgO powders are modeled using the Jones-Wilkins-Lee (JWL) equation of state, the Steinberg model and the Geologic Cap model, respectively. In the first case, the Jones-Wilkins-Lee (JWL) equation of state is used to link pressure to the specific volume, whereas the Steinberg plasticity model is suitable to model the steel tube, since it is designed for high strain rates simulating this way the loading conditions of the explosive compaction. The pressure, on the other hand, is determined by the Grüneisen equation of state as explained in Mamalis et al. (2011). The parameters of the Geologic Cap Model are fitted to the experimental data which are obtained by Nielsen et al. (2003). It should be noted, that the application of this model for low strain rates is made under the assumption that the material response will not be qualitatively different for high strain rate conditions, which is the case for the explosive compaction technique.

3 Model Optimization

The numerical simulation is a useful tool to obtain information about the testing conditions and to also monitor the temperature profile as well as the pressure and stresses applied to the PIT during the explosive compaction technique. It is therefore possible to modify the simulation procedure by determining the conditions that optimise the performance characteristics which are important for the quality of the final product. In this case the aim was to minimize the porosity of the compact which affects the critical current density of the material as discussed above.

3.1 Selection of Variables (inputs) and Performance Characteristics (outputs)

The first step of the optimization is the selection of variables (inputs) and performance characteristics (outputs). Between the numerous available variables of the numerical simulation, the external diameter of the tube d, the diameter of the PETN explosive D and the length of the PVC tube L which accommodated the explosive, and the PIT are selected as input parameters. On the other hand, the peak pressure p, the peak maximum principal stress s, the porosity f, the radius uniformity u, and the mass of the explosive m are the corresponding outputs which would determine the effectiveness of the optimization procedure. The outputs are calculated by processing the evolution versus time of the core circumference and core center pressure profiles, the maximum principal stress of the tube, the core volume change, and the tube radius reduction which are presented in Figures 2-5. The

pressure profiles in Figure 2 (a, b) are sampled in a series of elements located along the central axis, along the length and on the circumference of the core. The peak pressures and subsequently their averages are obtained from measurements performed during the transition of the initial shock front through the sample, for the time duration of 0 – 0.025 ms. It should be noted that according to the predictions of the finite element model, the maximum value of the peak pressure is recorded on the core circumference, reaching 5000 MPa. This is approximately two times higher than the corresponding peak pressure calculated at the core center which does not exceed 2500 MPa. It can also be observed that the maximum pressures produced by the incident compressive shock wave are measured as the front is approaching the bottom edge of the PIT (just before 0.0025 ms) which means that damping starts after the first reflection. On the other hand, the stresses are sampled on a series of elements along the length of the tube as shown in Figure 3, but in this case the calculations are conducted on the reflected wave (after 0.025ms) since the core material is considered to be still in powder form before the first reflection, indicating that the core cannot withstand any tensile stresses, not before it is fully consolidated. Again following a similar reasoning as before, the average of the maximum principle stresses is considered in the finite element model optimization.

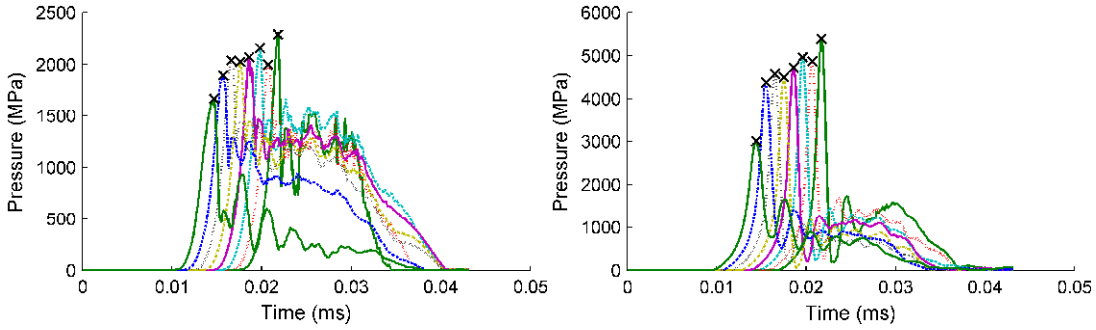

Figure 2. Pressure profiles and peak pressures measured at various locations (a) on the circumference and (b) at the center of the core

The volume change of the core and the radius reduction of the tube, which are used for the calculation of the porosity and the uniformity, are presented in Figures 4, 5. As expected, the volume of the compact is reduced as the initial compressive pulse travels through the core, reaching a minimum of 0.9 x 10^3 mm^3 at approximately 0.022 ms. The tube radius profile follows a similar pattern up to the first 0.022 ms, however the tube uniformity is reduced in the consequent stages of the simulation as indicated by the fluctuations that can be observed in the profiles.

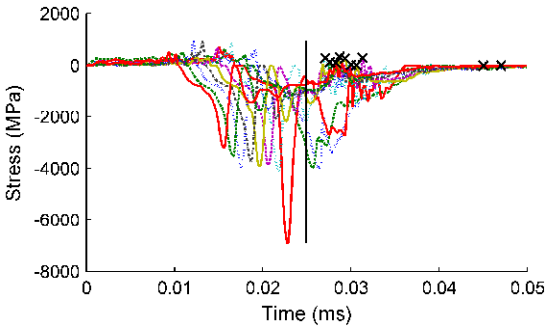

Figure 3. Maximum principal stresses along the length of the core measured after the first reflection of the shock wave

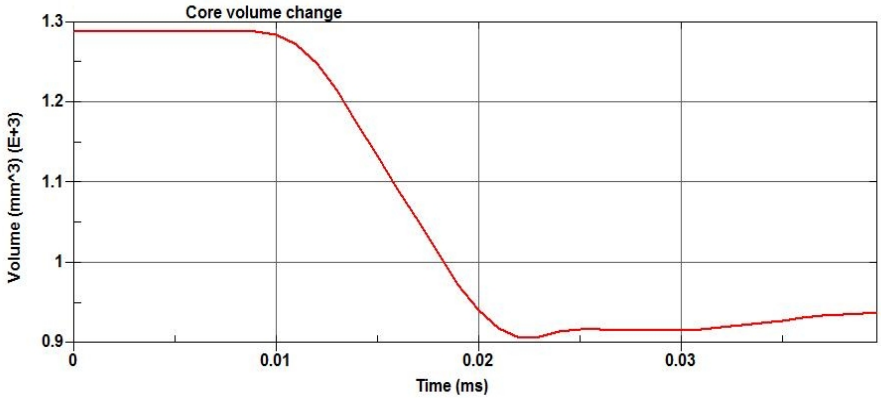

Figure 4. Core volume change imposed on the sample from the initial compressive shock front

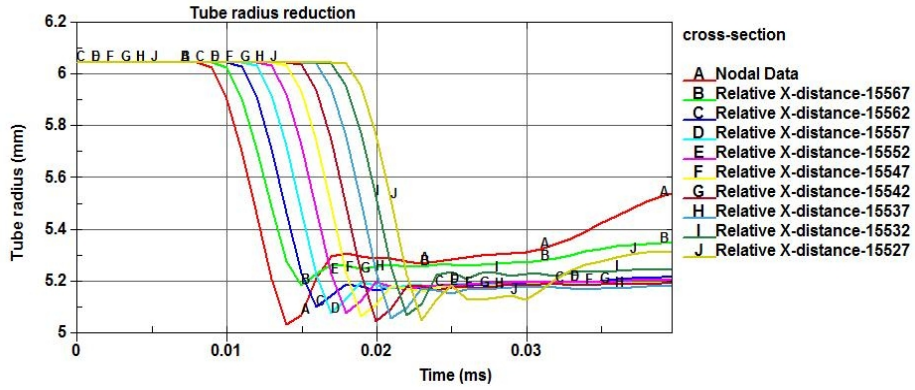

Figure 5. Tube radius reduction measured at the reference point and at various other locations at a certain distance from it

3.2 Initial Simulation Set Analysis

The initial simulation is carried out using L9 Taguchi design, which is immediately expanded to full factorial using 27 points and 7 variables for the ANOVA and response surface analyses as presented in Figures 6 (a-d) below. The plotmatrix in Figure 6 (a) is a graphical representation of all the different combinations between the inputs and the outputs of the numerical simulation, whereas the Analysis of Variance in Figure 6 (b) shows the interaction between them. It is obvious that the pressure p is the only magnitude which is dependent on the length L of the PVC container but at the same time it is independent of its diameter D. There are also no significant mixed effects that need to be considered in the calculations. The response surfaces in Figures 6 (c, d) are used to determine the optimal values of the peak pressure and porosity which in this case should be maximum and minimum, respectively.

The simulation results for the full factorial design including maximum, minimum and mean values as well as standard deviation are tabulated in Table 1. It may be suggested that the uniformity has a significantly low mean value which means that it may be neglected from the calculations. The relatively small standard deviation of the average peak pressure can also be observed, and, consequently, its weight was set to a low value in the objective function, as explained in detail below. This way the optimisation process may be focused mainly on the determination of the optimal peak stress and porosity which in turn have a high effect on the final product of the explosive compaction technique.

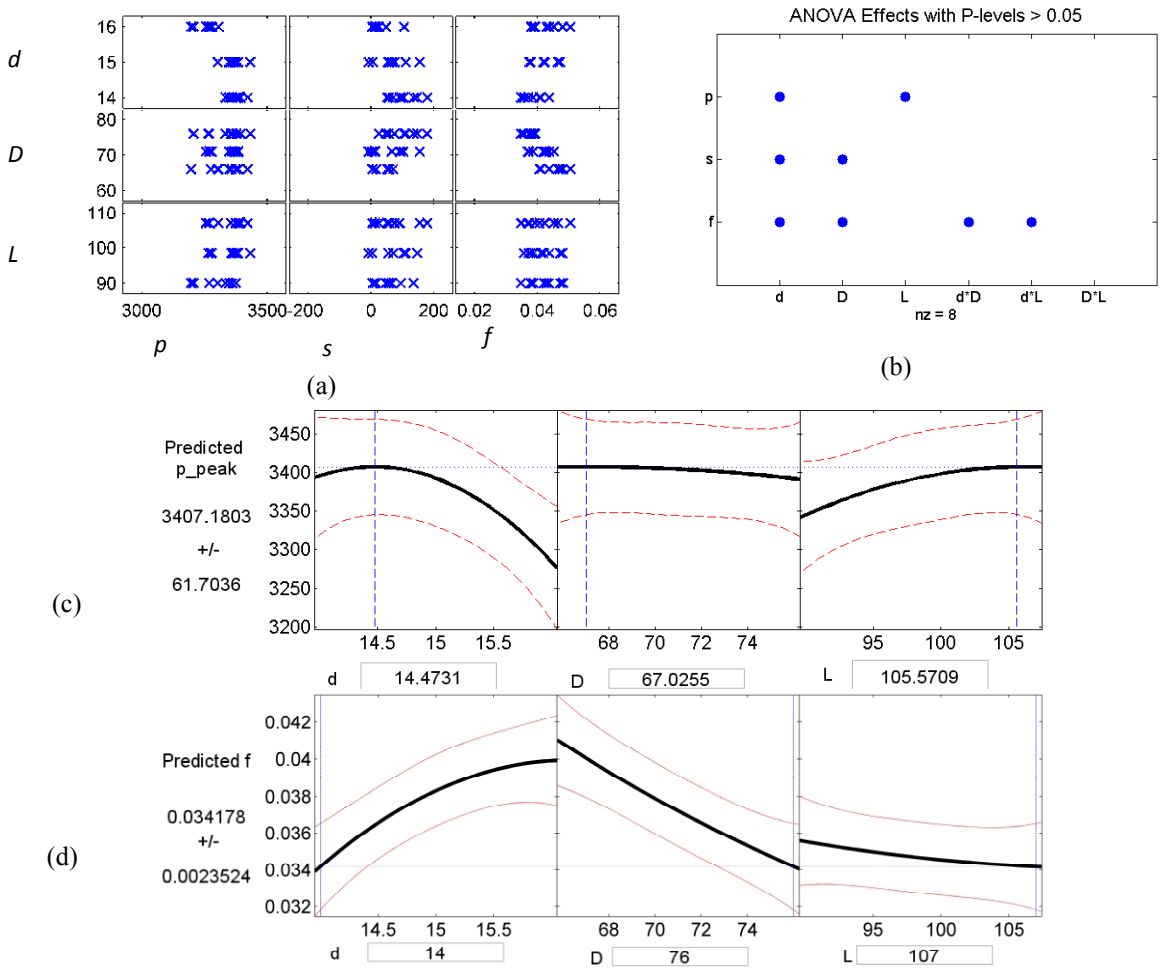

Figure 6. (a) Plotmatrix, (b) ANOVA, response surfaces for (c) peak pressure and (d) porosity

Full factorial design: 27 points	Pressure, p_peak (MPa)	Stress, s_peak (MPa)	Porosity, f	Uniformity, u (mm)	Explosive mass, m (g)
max	3432	179	5,05%	0,117	251,2
min	3197	-8	3,48%	0,054	87,7
std	62	52	0,45%	0,018	52,3
mean	3333	64	4,15%	0,086	160,6

Table 1. Results of the numerical simulation.

3.3 Non-Parametric Optimisation - Pareto Front

The Pareto front is the locus of experimental points, which may be found to be optimal under some choice of weights, whereas the points that do not belong to the front would never be optimal, regardless the choice of points; see the related theory in Kim et al. (2004). An optimisation which converges to the entire Pareto front rather than to a single point is called non-parametric. This technique has been utilised in similar problems as

explained in Soury et al. (2009), Wei et al. (2008), Sun et al. (2010). A good approximation of the Pareto front may be the basis for the application of a stochastic optimisation algorithm. It should be noted that any optimisation should always converge to a point on the Pareto front, and when it does not, its convergence should be considered as incomplete.

A meaningful multiparametric optimisation requires the selection of weights to be performed in a definitive fashion. It would be much more useful, however, to be able to quantify the tradeoffs that have to be made when selecting the weights, and how the optimum points will shift in relation to that. To this effect, utilising the simulated experimental points of the original full factorial design, the Pareto front is extracted for each case. Since the variation of the uniformity of the radius of the tube u is insignificant, it may be neglected limiting this way the number of the performance variables to three. This way, the problem can be easily reduced to 3x3 without compromising the effectiveness of the optimization. A more aggressive problem simplification can be carried out by decreasing the Pareto front to 2x2 as shown in Figures 7 (a, b), where the maximum principal stress s and the length of the PVC container L are not taken into account. It is worth mentioning that the techniques which were implemented to determine the net generation of the simulation points are the vertices of the Voronoi cells, centered at the Pareto front together with their neighbouring points. The middle points of the Delaunay triangle faces of the Pareto front are also included as graphically illustrated in Figure 7(a). On the other hand, the steep shape of the optimal curve in Figure 7(b) implies that there is only a limited number of tradeoffs between porosity and peak pressure. It may be suggested that the optimization is completed when the density of points in the variable space inside the tessellated area reaches a limit. This limit is dictated by simple engineering considerations, and in this case d is equal to 0.25 mm whereas D and L are equal to 1 mm.

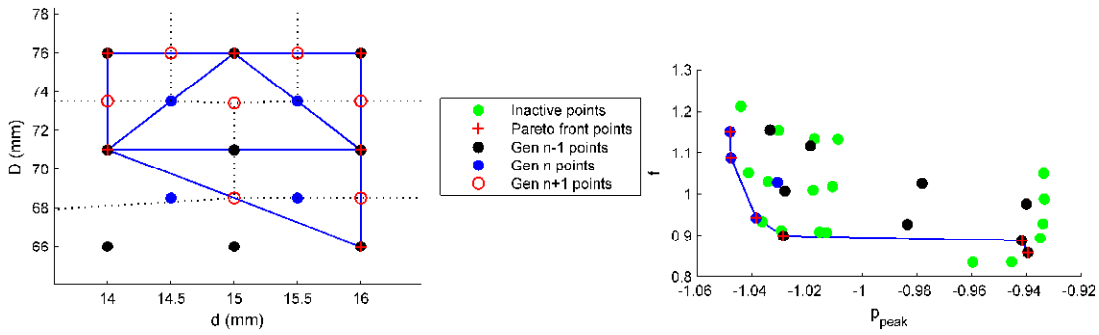

(a) (b)

Figure 7. Pareto front 2x2, considering p and f to be functions of d and D: (a) Variable space; (b) Performance space.

The 3x3 Pareto front in the performance and variable spaces including the external diameter of the tube d, the diameter D and the length L of the PVC container which are used for the optimisation of the peak pressure p, the principal stress s, and the porosity f is presented in Figures 8 (a, b). In this case, the Pareto front surface is fitted with an interpolant (cubic spline). It may also be suggested by observing the shape of the Pareto front in Figure 8 (a) that compared to the optimisation of the pressure and the principle tensile stress, improvements in the porosity level of the compact are easier to be made. On the other hand, the tessellation of the Pareto front points in the variable space, as presented in Figure 8 (b), provides the approximate area in which the optimal designs exist.

A different optimisation scheme which considers the production cost by including the mass of the explosive m into the performance space is presented in Figures 9 (a, b). The results here are only indicative, since the experimental set has not been expanded to cover the vicinity of the Pareto front points in the variable space. As shown, most of the expanded set points from the previous optimisation fall outside the tessellated area.

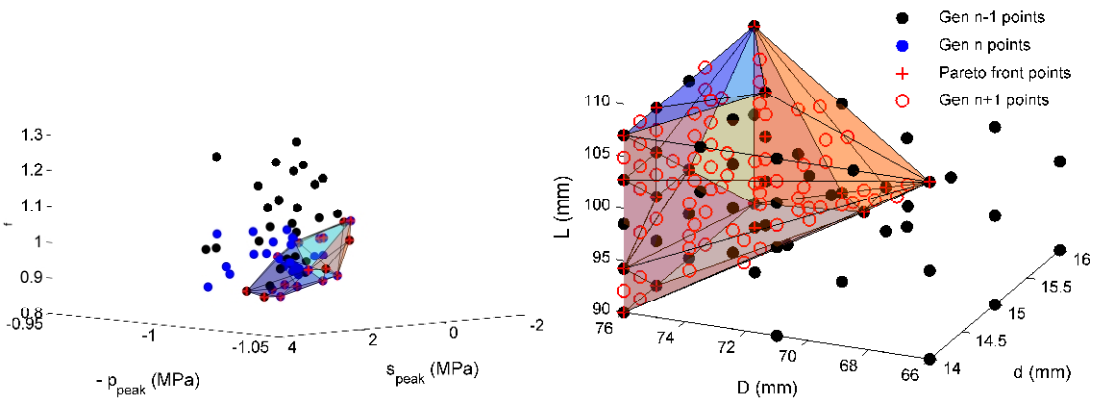

(a) (b)

Figure 8. Expanded 3x3 Pareto front, including *p, s, f, d, D* and *L*: (a) Performance space; (b) Variable space.

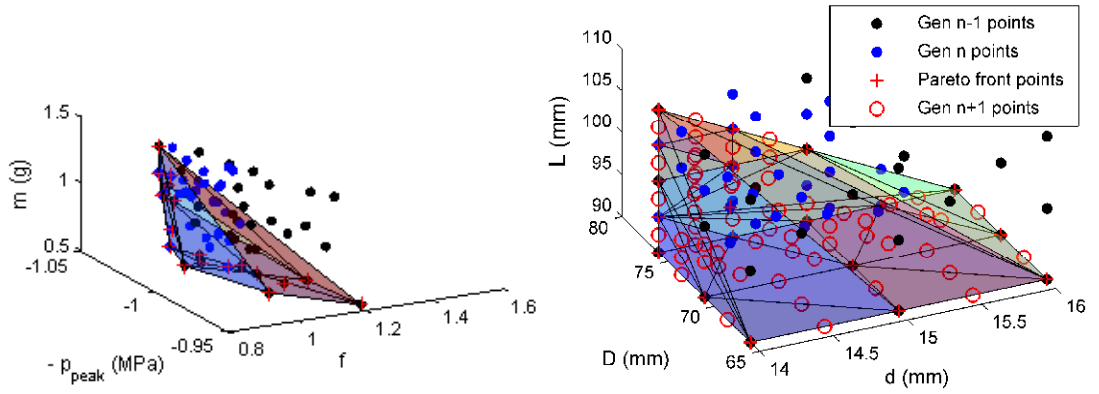

(a) (b)

Figure 9. Modified 3x3 Pareto front, considering the production cost by including the mass of the explosive in the performance space: (a) Performance space; (b) Variable space.

3.4 Determination of the Objective Function

The selection of weights that are used in the objective function was based on the variance of each performance characteristic and the shape of the Pareto front. To each output is assigned a specific weight value depending on the effect that it has on the final product of the forming procedure. In particular, the weight that corresponds to the peak pressure was set to w_1=0.1, due to the small scale variations observed in the measurements, whereas the peak stress was given a larger value, w_2=0.2, since it is considered to be a performance characteristic of higher importance. Porosity as discussed above is the most important parameter to optimise. Therefore, its weight value was set to w_3=0.5. Uniformity on the other hand has a very low standard deviation and, therefore, the choice of the weight value is w_4=0. Finally the mass of the explosive is given a weight of w_5=0.2 since it is an output of similar importance to the peak stress.
Once the weights are selected, an objective function combining all the outputs which is normalised by dividing with their average values taken from Table 1 is constructed, as shown in equation (1), and subsequently a response surface optimisation of this function is performed.

$$I = -w_1 \cdot \frac{p}{\bar{p}} + w_2 \cdot \frac{s}{\bar{s}} + w_3 \cdot \frac{f}{\bar{f}} + w_4 \cdot \frac{u}{\bar{u}} + w_5 \cdot \frac{m}{\bar{m}} \quad (1)$$

Based on the above, a new quadratic response surface is calculated from all the available points, and the optimum is determined.

4 Results and Discussion

The results obtained from the numerical simulation before and after the completion of the optimisation are presented in Table 2 shown below. The "initial" row represents the output of the first simulation. The set "All" corresponds to the total number of runs performed where the average value of the corresponding measurements is displayed. The next set "FF" are the runs of the Full Factorial, and the remaining points except that of the initial set are denoted by "FU". The "Pareto" set are the optimal points of the "FF" and "FU" sets. The "RSM-p", "RSM-s" and "RSM-f" rows correspond to the optimisation performed using the Response Surface Method with respect to the peak pressure, principal stress, and porosity, respectively, aiming for individual optimisation, where the optimal of each parameter is obtained. The last row of Table 2 displays the final results of the optimisation after the construction of the multiparametric objective function.

Set	Points	Pressure p_peak (MPa)	Stress s_peak (MPa)	Porosity f	Uniformity u (mm)	Charge mass m (g)
Initial	1	3368	-8	4,20%	0,093	160,1
All (avg)	66	3348	78	3,99%	0,080	171,5
FF (avg)	27	3333	64	4,15%	0,086	160,6
FU (avg)	39	3359	87	3,88%	0,076	179,0
Pareto (avg)	19	3349	68	3,99%	0,078	172,8
RSM-p	1	3197	179	5,05%	0,117	187.2
RSM-s	1	3405	-484	2,74%	0,138	87.7
RSM-f	1	3405	5	3,95%	0,112	251.2
Final	1	3206	48	3,80%	0,087	117,1

Table 2. Tabulated results of the numerically optimised explosive compaction technique

5 Conclusions

Summarising the main results pertaining to the optimisation of the explosive compaction of MgB_2 using the PIT method, it may be concluded that under the assumptions made in the numerical model, using the geologic cap model for high strain rate phenomena, the predictions of the optimisation process show a divergence from the results obtained from the theoretically designed compaction process. In particular:

(a) The peak pressure and the porosity can be independently optimised by varying the length and the diameter of the PVC container which accommodates the PIT and the explosive.
(b) The soundness of the compacts is affected by the quantity of the high explosives used.
(c) The radii variation of the compacts is insignificant and, therefore, their optimisation can be omitted.

Note that the porosity of the sample is considered to be the most important parameter since it affects the superconducting performance of the material. According to the predictions of the optimised simulation models the porosity of the compact reaches approximately 3.8 percent, which is relatively lower compared to the porosity level 4.2 percent that was calculated by the initial non-optimised model.

References

Mamalis A. G.; Hristoforou E.; Manolakos D. E.; Prikhna T.; Theodorakopoulos I. D.; Kouzilos G.: Explosively Consolidated Powder-In-Tube MgB_2 Superconductor Aided by Post-Thermal Treatment, *IEEE Transactions on applied superconductivity,* 19, (2009), 20-27.

Mamalis A. G.; Theodorakopoulos I. D.; Vortselas A. K.: Numerical Simulation of Explosively Compacted Powder-In-Tube MgB_2 Superconductor, *Material Science Forum*, 673, (2011), 131-136.

Nielsen M. S.; Hancock M. H.; Eriksen M.; Bech J. I.; Bay N.: Comparison of the yield properties of Magnesium Di-Boride and BSCCO precursor powder, *Proc. 24th RISØ International Symposium on Materials Science*, (2003), 81-82.

Kim I.Y.; de Weck, O.L.: 2005. Adaptive weighted-sum method for bi-objective optimization: Pareto front generation, *Struct. Multidisc. Optim*., 29, (2005), 149-158.

Soury E.; Behravesh A.H.; Rouhani Esfahani E.; Zolfaghari A.: Design, optimization and manufacturing of wood–plastic composite pallet, *Materials and Design*, 30, (2009), 4183–4191.

Wei L.; Yang Y.; Multi-objective optimization of sheet metal forming process using Pareto-based genetic algorithm, *J. Mater. Proc*,. 208, (2008), 499-506.

Sun G.; Li G.; Gong Z.; Cui X.; Yang X.; Li, Q.: Multiobjective robust optimization method for drawbead design in sheet metal forming, *Materials and Design*, 31, (2010), 1917–1929.

Addresses: Academician Prof. Dr-ing, Dr.h.c. Prof.h.c Athanasios G. Mamalis, Project Center for Nanotechnology and Advanced Engineering, National Center of Scientific Research "Demokritos", 15310 Agia Paraskevi, Athens, Greece. Dipl.-Ing. Ioannis D. Theodorakopoulos and Dipl.-Ing. Achilleas Vortselas, Manufacturing Technology Division, Mechanical Engineering Department, National Technical University of Athens, Iroon Polytechniou 9, 15870 Zografou, Athens, Greece.
email: *mamalis@ims.demokritos.gr; johnlanc@hotmail.com; vortse@gmail.com*